Shapes, wavelength selection, and the cellular-dendritic "transition" in directional solidification

P. Kurowski, C. Guthmann, and S. de Cheveigné
Groupe de Physique des Solides, Université de Paris VII, 2 Place Jussieu, 75251 Paris CEDEX 05, France
(Received 18 July 1990)

We have studied cellular shapes in directionally solidified CBr_4-Br_2 and have shown that they follow a scaling law from the planar-cellular threshold V_c up to about $(8-9)V_c$: the shapes depend on the *relative* velocity $\epsilon=(V-V_c)/V_c$, and not separately on the absolute velocity V or the temperature gradient G. A comparison with Saffman-Taylor profiles is found to be unsatisfactory. We then examined cellular widths and their variation along a given solidification front from threshold up to the appearance of dendrites. Again up to about $(8-9)V_c$, the dispersion is comparable to experimental uncertainties but beyond that point the width of some cells begins to increase spectacularly. These abnormally wide cells change shape, and the widest ones become dendrites once the Péclet number reaches 2–3.

I. INTRODUCTION

The growth forms of crystals are often spectacularly regular. They are the result of a dynamical balance between the production of latent heat—and of solute in the case of alloyed materials—and their evacuation away from the solid-liquid interface.[1] Here, we shall examine the patterns exhibited by the interface between solid and liquid during directional solidification. In this experiment, the sample (a thin sample of a transparent organic containing a small solute concentration C_0), initially liquid, is pulled at a given speed V in an imposed temperature gradient G set up around its melting temperature. Below a critical pulling velocity V_c (for a given concentration and temperature gradient), the solid-liquid interface is planar. Above, it presents a quasiperiodic cellular deformation (on a scale of the order of 50 μm) the amplitude of which increases with increasing pulling speed. The cells eventually develop sidebranches, (at V of the order of $10V_c$ in the material under investigation here) and are then called dendrites. These patterns are related to solute segregation in the solid.

Mullins and Sekerka[2] analyzed the physical mechanism of the instability that results from the competition between the destabilizing effects of the solute diffusion and the stabilizing effects of the temperature gradient and of the interfacial tension. In the limit of low velocities and for materials with equal heat conductivities in the solid and in the liquid, the bifurcation from a planar to a cellular front takes place at a critical velocity

$$V_c=\frac{DGK}{m(K-1)C_0}$$

where D is the solute diffusion constant in the liquid, m is the liquidus slope, and K is the partition coefficient of the alloy.

Since then, interest in solidification has grown among physicists in the perspective of the study of systems far from equilibrium in which a periodic pattern develops, such as in Rayleigh-Bénard convection[3] or Taylor-Couette flow.[4] The same type of general questions appear: is the period well defined? how is it selected? does a unique and reproducible value appear, or does it depend on the history of the system?

In the present paper we first examine cellular shapes in CBr_4-Br_2 and show that they follow a scaling law from V_c up to about $(8-9)V_c$: the shapes depend on the *relative* velocity $\epsilon=(V-V_c)/V_c$, and not separately on absolute velocity V or temperature gradient G. We then consider widths of individual cells along a given interface and their dispersion from threshold up to the appearance of dendrites. Again up to about $8V_c$, the cellular width is well defined, the dispersion being comparable to experimental uncertainties but beyond that point the width of some cells begins to increase spectacularly. These abnormally wide cells change shape; the widest ones become dendrites once the Péclet number reaches 2–3.

II. EXPERIMENT

The experimental setup is essentially similar to that suggested by Jackson and Hunt[5] and has been described elsewhere.[6] The alloy studied is CBr_4 with 0.12% impurities, essentially Br_2. The material is chosen because it is a plastic crystal that, like most metals, presents a solid-liquid interface that is rough on the atomic scale. The solidification kinetics are expected to be rapid, the interface to be locally at a thermodynamic equilibrium, and indeed the solid does not facet. Physico-chemical constants for the alloy are to be found in Ref. 6. The samples are approximately 50 μm thick which excludes convection in the liquid phase. The experiments take place under the microscope and are video-taped. Selected frames are digitalized (512×760 pixels$\times256$ gray levels) on a MacIntosh II microcomputer and cell contours are extracted and analyzed.

In these experiments only cells or dendrites oriented perpendicular to the solid-liquid interface were retained. All the states were stationary on the time scale of our experiments, which decreased from several hours to several

minutes as pulling velocity is increased over the range studied here (2–70 μm/s). These times are well above the characteristic solute diffusion times [D/KV^2 in (s) $\sim 10^4/V^2$ (in μm/s)].

During an experiment, the pulling speed is increased by small steps ($\approx 10\%$ of the final speed).[7]

III. CELL SHAPES

As the pulling velocity is increased above threshold (for given concentration and temperature gradient) the cells become deeper and more pointed (Fig. 1) and their width decreases[6] as $V^{-0.4\pm0.1}$. They nevertheless retain a more or less rounded[8] shape, as opposed to more pointed forms which we shall discuss below. These cells, which exist up to about ten times threshold, have a number of common characteristics.

The most obvious parameters with which to characterize cell shapes are the cell width λ and the tip radius ρ. The ratio of the two, the reduced tip curvature λ/ρ, measures the "pointedness" of the cell.[9] We measure the cell width directly, taking the distance between midpoints be-

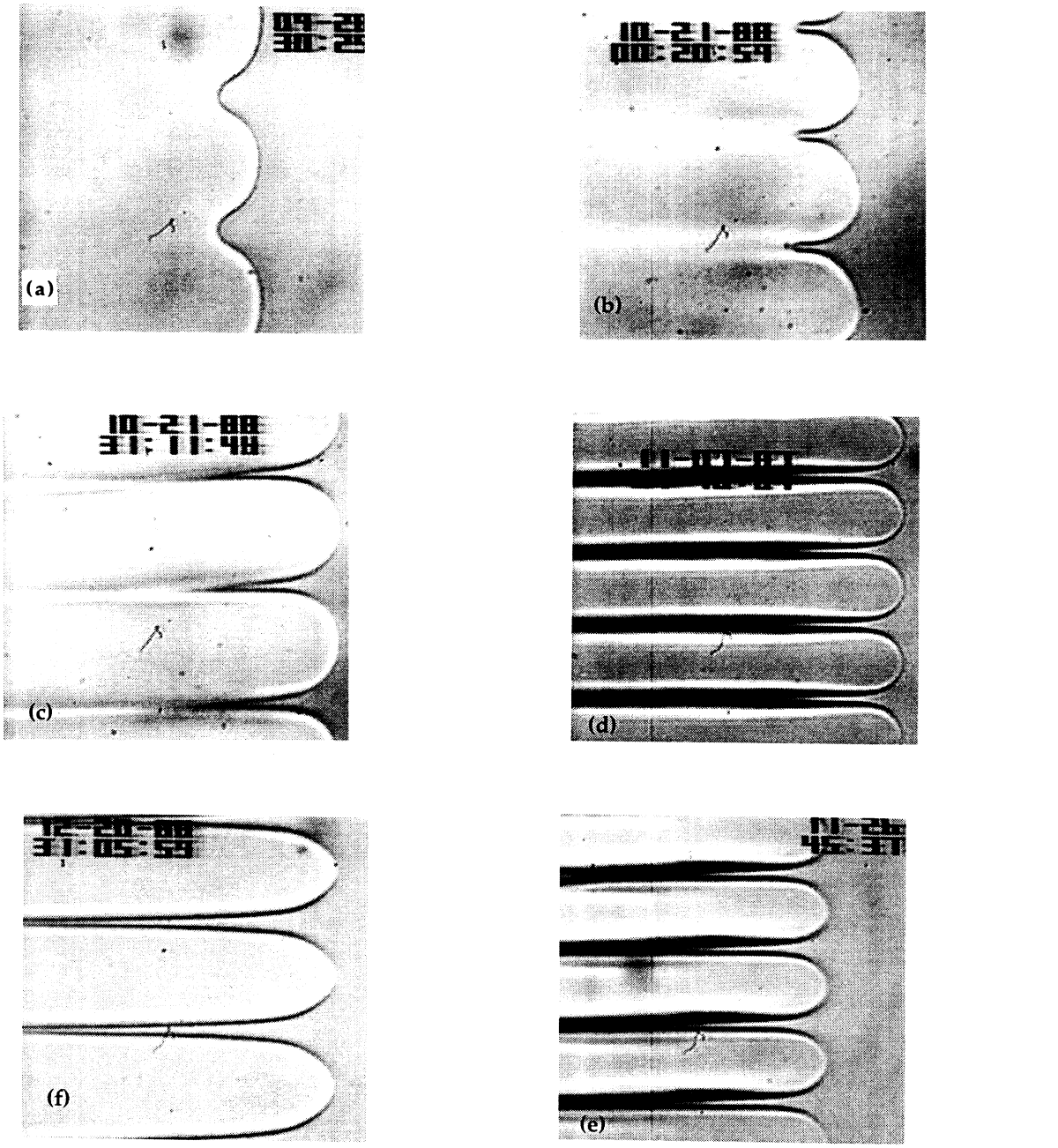

FIG. 1. Cell shapes for different relative velocities: (a) $\epsilon \approx 0.3$ ($V = 7.4$ μm/s, $V_c = 6$ μm/s, $G = 110$ K/cm, $\lambda = 55$ μm, $P = 0.35$); (b) $\epsilon \approx 1.6$ ($V = 14$ μm/s, $V_c = 5.4$ μm/s, $G = 110$ K/cm, $\lambda = 45$ μm, $P = 0.5$); (c) $\epsilon \approx 2$ ($V = 16.6$ μm/s, $V_c = 5.4$ μm/s, $G = 107$ K/cm, $\lambda = 40$ μm, $P = 0.6$); (d) $\epsilon \approx 4$ ($V = 25$ μm/s, $V_c = 5$ μm/s, $G = 106$ K/cm, $\lambda = 30$ μm, $P = 0.6$); (e) $\epsilon \approx 7.5$ ($V = 31$ μm/s, $V_c = 4.1$ μm/s, $G = 100$ K/cm, $\lambda = 30$ μm, $P = 0.8$); (f) $\epsilon \approx 8.5$ ($V = 49.3$ μm/s, $V_c = 5.3$ μm/s, $G = 110$ K/cm, $\lambda = 45$ μm, $P = 1.9$).

tween adjacent cells (precision 2–3%) and the tip radius is obtained by fitting the tip to a parabola (Fig. 2, precision 5%). The height h at which the tip deviates from the parabola is smaller or of the order of the tip radius: h/ρ varies from about 0.25 near threshold to about 2 at $10V_c$. Surprisingly, whatever the shape of the cell, the width w over which the fit is good is approximately two-thirds of the cell width.

Along a given front, one can observe some dispersion in cell widths (this dispersion is discussed below). The tip radii are also different, yet the ratio λ/ρ is constant to within less than 10% (Figs. 3 and 4). What is more, the cells are homothetic, i.e., they are superposable when reduced to unit width (Fig. 5). The cell shape is given under a given set of values of the control parameters. Yet when one compares experiments with different thresholds (due here to the use of different temperature gradients) shapes are very different for equal velocities. On the other hand, they are identical for equal *relative* velocities $\epsilon=(V-V_c)/V_c$. Figure 6 shows the superposition of two such cells. Figure 7 shows that the ratio λ/ρ (averaged along a given front) increases as ϵ increases: the cells become more pointed. We thus find the following scaling law: in the range of parameters explored, cell shapes depend only on the parameter ϵ and not on V or G separately.

No exact analytic predictions of cell shapes exist up to now: the system under study is highly nonlinear since we are working well above the planar-cellular bifurcation (which is subcritical[6] in CBr_4-Br_2), so amplitude equation methods are not applicable. In the small-Péclet-number approximation, i.e., when the diffusion length $l_D=D/V$ (D is the solute diffusion coefficient in the liquid) is much greater than the cell width λ ($P=\lambda/l_D \ll 1$), an approximate analytic treatment of the directional solidification (DS) problem can be carried out because it becomes formally analogous to the Saffman-Taylor (ST) problem.[10–13]

When this analogy is made between the two problems,

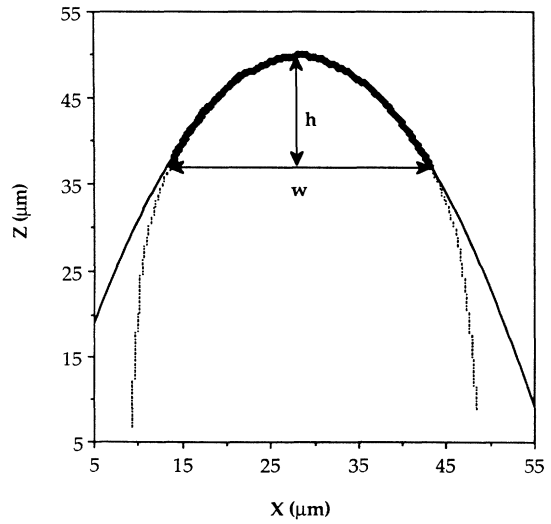

FIG. 2. Fit of the cell tip (overlapping squares) to a parabola (solid line). The base of the cell is in fine dots.

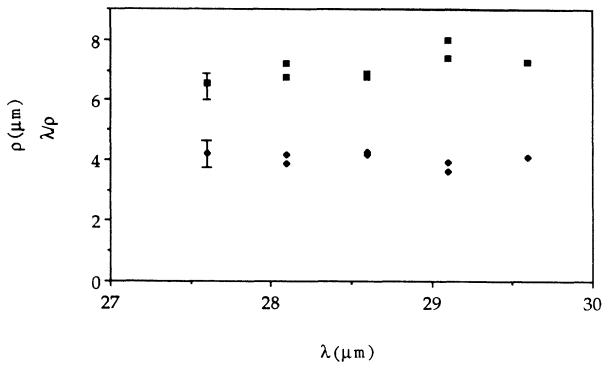

FIG. 3. Tip radius ρ (squares) and reduced curvature λ/ρ (diamonds) vs cell width ($G=104$ K/cm, $V=30$ μm/s, $\epsilon=5.5$).

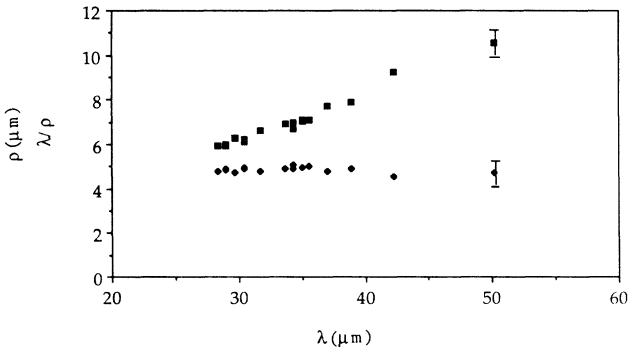

FIG. 4. Tip radius ρ (squares) and reduced curvature λ/ρ (diamonds) vs cell width ($G=104$ K/cm, $V=45$ μm/s, $\epsilon=8.5$).

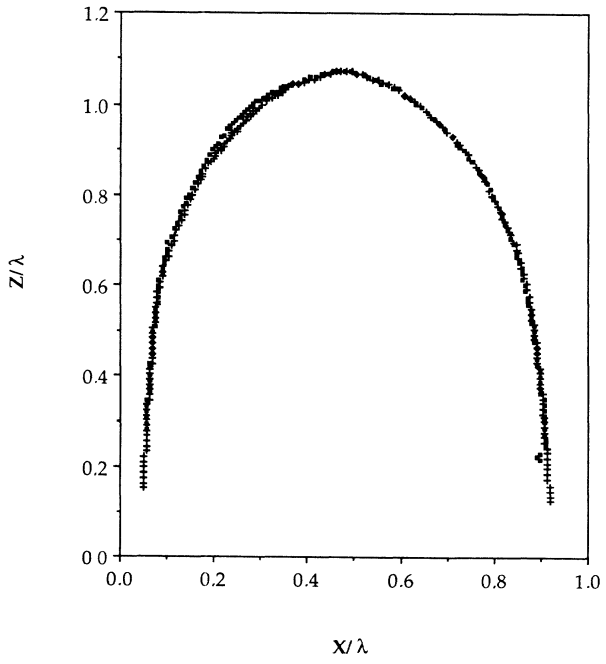

FIG. 5. Superposition of two cells of different widths taken from the same front and reduced to unit width ($G=110$ K/cm, $V=49$ μm/s, $\epsilon=8.3$). Squares, $\lambda=41$ μm; crosses, $\lambda=46$ μm.

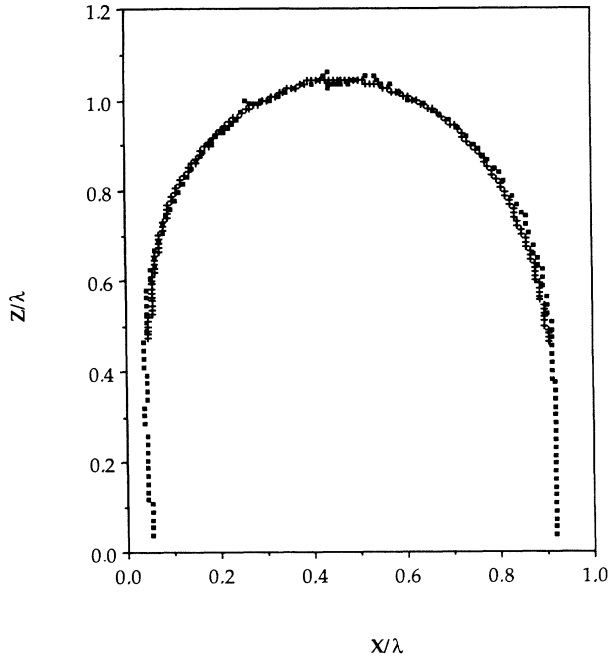

FIG. 6. Superposition of two cells taken from different experiments carried out at the same relative velocity ϵ, and reduced to unit width. Squares: $G=100$ K/cm, $V=30$ μm/s, $\lambda=29$ μm, $\epsilon=5.5$, $\lambda/\rho=3.6$; crosses: $G=46$ K/cm, $V=21$ μm/s, $\lambda=36$ μm, $\epsilon=5.5$, $\lambda/\rho=3.6$.

an effective surface tension coefficient σ_{eff} appears. [The equivalent parameter in the ST problem is $\sigma_{\text{ST}}=b^2T/(48\mu Ua^2)$ where b is the Hele-Shaw plate spacing, a its half width, μ the viscosity of the driven fluid, U the velocity of the interface, and T the surface tension.] In directional solidification it has been shown by Mashaal *et al.*[14] to be

$$\sigma_{\text{eff}}=\frac{1-(1-K)\lambda_{\text{ST}}}{K}\frac{\sigma}{\epsilon},$$

where K is the solute partition coefficient, λ_{ST} the relative width of the Saffman-Taylor finger that fits the tip of the cell, and σ is the capillary constant $\sigma=d_0l_t/\lambda^2$. Here d_0 is the capillary length, which characterizes the length scales on which capillarity stabilizes the solid-liquid interface: $d_0=T_M\gamma K/[C_0(K-1)mL]$ where T_M is the melting temperature of the pure material and γ is the surface tension; l_t is the thermal length, characterizing the length scale on which the temperature gradient G stabilizes the interface: $l_t=C_0(K-1)m/(KG)$.

Our experiments could eventually satisfy the low-Péclet-number condition (our minimum $P\approx0.4$), so we have carried out the comparison. For CBr_4-Br_2, $d_0=4\times10^{-6}$ cm, $l_t(\text{cm})=1.8/[G(\text{K/cm})]$, so $\sigma=730/\{[G(\text{K/cm})][\lambda^2(\mu\text{m}^2)]\}$.[15] A typical order of magnitude for σ will be therefore 10^{-3}–10^{-2} while σ_{eff} will vary in the range 10^{-4}–10^{-2} (since $\lambda_{\text{ST}}\approx0.5$–1). These are small values: the corresponding ST fingers with such surface tension coefficients have relative widths between 0.5 and 0.6 and relative tip curvatures greater than 4.5 (except in presence of anisotropy[16] where the relative widths are even smaller and the curvatures larger). This does not correspond to the range observed in DS experiments (Fig. 7).

DS cells should be compared to the ST profiles *in the presence of interfacial tension* that have been calculated numerically by MacLean and Saffman.[17] Their relative width λ_{ST} is determined by requiring the relative tip curvature of the finger profile to be equal to that of the measured cell. The shapes closest to threshold [Figs. 1(a) and 1(b)] are squarer than any shape observed in the ST experiment, perhaps due to the influence of the cell cusps that are very shallow. Figure 8 shows a DS cell ($\epsilon=5.5$, $P=0.7$) and the ST shape ($\lambda_{\text{ST}}=0.79$) of same relative tip curvature. (Note that the shapes coincide over a height much smaller than the cellular width.) For this cell $\sigma_{\text{eff}}=3.4\times10^{-3}$ whereas the surface tension coefficient

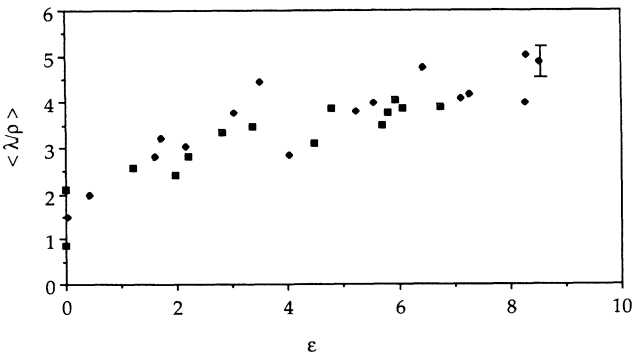

FIG. 7. Average value of the reduced curvature λ/ρ along a given front vs relative velocity ϵ (squares, $G=50$ K/cm; diamonds, $G=100$ K/cm).

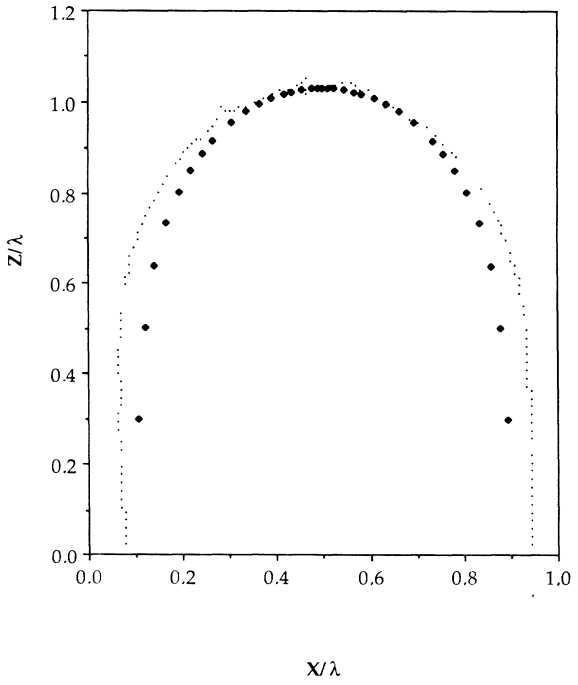

FIG. 8. Superposition of a Saffman-Taylor profile (squares, $\lambda_{\text{ST}}=0,79$) and a solification cell (dots, $G=100$ K/cm, $V=30$ μm/s, $\lambda=29$ μm, $\epsilon=5.5$, $\lambda/\rho=3.3$, $P=0.7$).

for a ST finger of relative width 0.79 is $\sigma = 6 \times 10^{-2}$. The same process with a more pointed DS cell ($\epsilon = 8.5$, $P = 1.1$) gives a ST finger of $\lambda_{ST} = 0.6$, $\sigma_{eff} = 3.3 \times 10^{-3}$ and $\sigma = 5 \times 10^{-3}$. Table I is the result of a number of such comparisons. Clearly, the surface tension parameters are not equivalent.

It would seem, therefore, that at the values of the Péclet number at which our experiments are carried out, the formal analogy between ST and DS equations no longer holds. Numerical calculations by Mashaal and Ben Amar[18] clearly illustrate this point. At $P = 0.6$ they attain a regime where the relative curvature is practically independent of λ_{ST} (which they calculate by fitting the sides of the cells, not the tip) and is close to the value ($\lambda/\rho = 2$) which we observe at the same relative velocity $\epsilon = 2$. Experimentally, it will not be easy to go to a lower-Péclet-number regime since P varies roughly as $V^{1/2}$: dividing P by 10 implies dividing pulling speeds by 100.

A number of authors have performed numerical calculations of cellular shapes.[19–22] Saito *et al.*[23] have performed dynamical calculations of cell shapes for our material, under the same conditions of velocity, temperature, gradient, and wavelength. A superposition of the experimental and predicted numerical profiles is shown in Fig. 9. The agreement is good (consider the variety of shapes observed experimentally, Fig. 1), although a systematic discrepancy is observed: the tip radii of the calculated profiles (in Fig. 9, $\rho_{num} = 4.5$ μm and $\rho_{expt} = 6.5$ μm) are smaller than the experimental ones. We attribute this to the fact that the calculations are carried out in two dimensions whereas the experiments are three dimensional. (We have previously proved the importance of the third dimension both in displacing the threshold due to the curvature of the solid-liquid meniscus,[6] and in the capillary instability of cell cusps.[24] Effects of the third dimension have also been observed in Saffman-Taylor fingers by Tabeling *et al.*[25]) By measuring the curvature of the projection of the cell tip onto the plane of the sample we miss the component of the curvature in the perpendicular direction. Since the sample thickness is of the same order as the cell width, the measured curvature could be a factor of the order of 2 smaller than the total curvature. On the other hand, in the numerical profiles, the total curvature is in the two dimensions. We feel that these results show that it is somewhat illusory to seek for a precise fit between two-dimensional (2D) calculations (numerical or analytical—such as in the Saffman-Taylor model described above) and experiments carried out in thin samples, the third dimension of which is clearly important.

TABLE I. Relative velocity ϵ, Péclet number P, width λ_{ST} of the Saffman-Taylor finger of equal relative tip curvature, effective surface tension parameter σ_{eff}, and expected ST surface tension parameter σ_{ST} for different cells.

ϵ	P	λ_{ST}	σ_{eff}	σ_{ST}
10.5	1.1	0.6	3.3×10^{-3}	7.4×10^{-3}
4.8	0.6	0.68	3.4×10^{-3}	2.2×10^{-2}
5.5	0.7	0.78	3.4×10^{-3}	5.4×10^{-2}
5.5	0.9	0.85	1.8×10^{-3}	8.6×10^{-2}
4	0.6	0.94	2.6×10^{-3}	1.7×10^{-1}

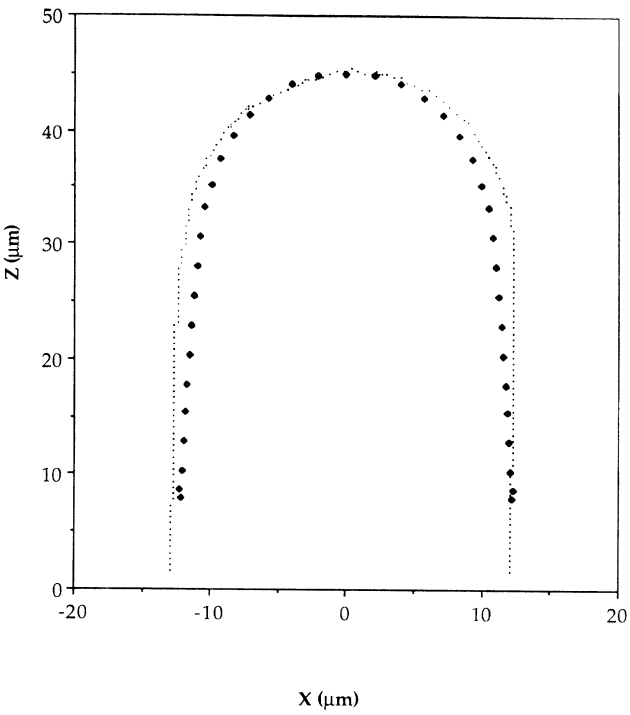

FIG. 9. An experimental profile (dots, $G = 100$ K/cm, $V = 31$ μm/s, $\lambda = 29$ μm, $\epsilon = 5$) and the profile calculated numerically by Saito *et al.* for the same conditions (diamonds).

IV. WAVELENGTH DISPERSION

The morphology of a solidification front in the cellular regime (i.e., up to relative velocities $\epsilon \approx 7-8$), once a stationary state is reached, is to a good approximation periodic and the wavelength measured is usually an average over several tens of cells—we note it here as $\bar{\lambda}$. But in the present study we are particularly concerned with the dispersion around this value. We shall therefore consider the widths of individual cells, noted λ.

Figures 10 and 11 show the widths of individual cells versus pulling velocity for two temperature gradients ($G = 50$ and 100 K/cm): points on a vertical correspond to cells along a given front. The straight lines represent the variation of the average wavelength $\bar{\lambda}$ as previously reported.[6] In the cellular regime, $\bar{\lambda}$ decreases as $V^{-0.4 \pm 0.1}$, with a standard deviation on λ less or of the order of 10%. The experimental sources of fluctuations in cell widths are of the same order. These are due to irregularities in pulling speed which give a $\delta\lambda/\bar{\lambda} \approx 3\%$; side and grain boundary effects can give a $\delta\lambda/\bar{\lambda} \approx 5\%$; irregularities in temperature gradient and thickness give a negligible $\delta\lambda/\bar{\lambda}$.[7] Because of this experimental "noise," we cannot affirm that there is strict selection of λ, but the band of wavelengths observed is very narrow in comparison to the width of the Mullins and Sekerka[2] neutral curve or even to the Eckhaus limit (calculated so far only for a normal bifurcation[26]).

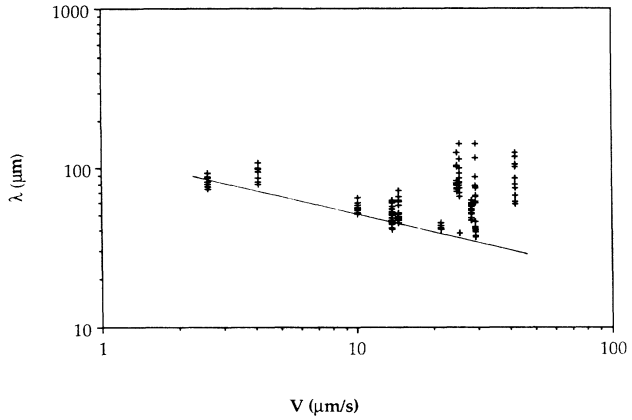

FIG. 10. Cell width λ vs pulling velocity V for a temperature gradient $G \approx 50$ K/cm. $V_c = 2.7$ μm/s. The straight line represents previous results (Ref. 6) concerning the average wavelength.

Beyond a certain velocity, the dispersion in cellular widths begins to increase spectacularly. It is to be noted that the points are spread *above* the $V^{-0.4}$ curve: anomalously wide cells are appearing. The increase in dispersion takes place at different velocities in Figs. 10 and 11 but *at the same relative velocity*: $\epsilon \approx 7-8$.

In the cellular regime wavelength adjustment can take place via local phenomena such as cell splitting or pinching off.[6,7] The widths of neighboring cells then adjust progressively by what could be a phase diffusion mechanism. The phenomenon is illustrated in Figs. 12(a), a photograph of the solid shortly after the pinching off of a cell, and 12(b) and 12(c) which show the evolution of the cell widths with time during the same event. The width adjustment is only measureable over 2–3 cells, a distance insufficient to allow a quantitative analysis that could distinguish between diffusion and propagation.

As the relative velocity is increased, the cells continue to be pinched off but splitting no longer takes place. The

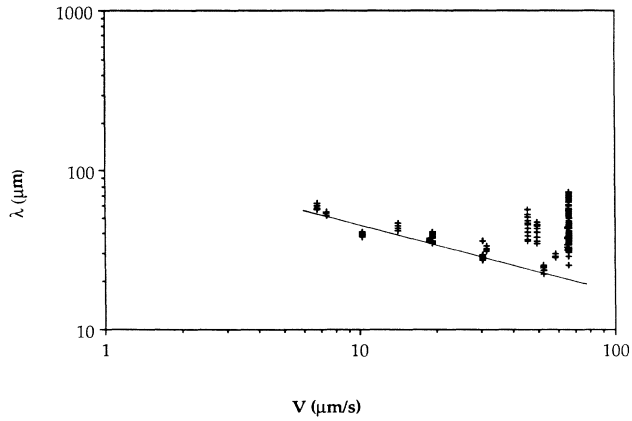

FIG. 11. Cell width λ vs pulling velocity V for a temperature gradient $G \approx 100$ K/cm. $V_c = 5.4$ μm/s. The straight line represents previous results (Ref. 6) concerning the average wavelength.

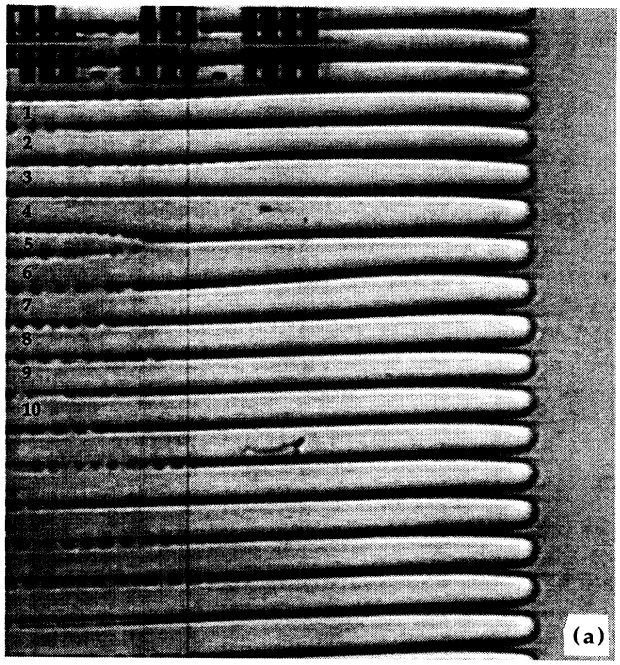

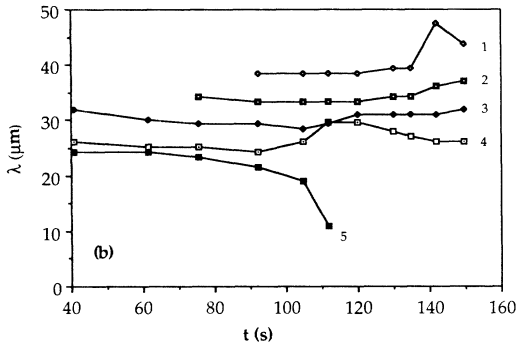

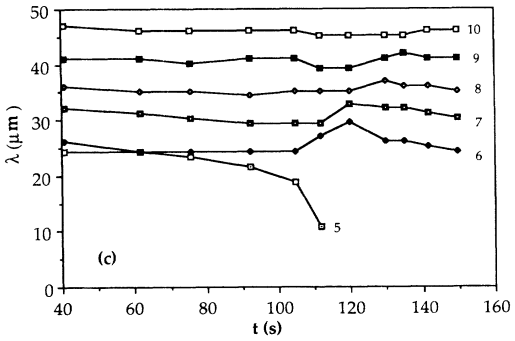

FIG. 12. A cellular front shortly after the pinching off of a cell (a) and (b), (c) the evolution in time of the widths of the cells numbered in Fig. 13(a). Cell number 5 is pinched off at time $t \approx 110$ s. Its neighbors become successively abnormally wide then readjust on a time scale of the order of a minute.

cell tip radius having decreased, a much greater fluctuation of tip curvature is necessary to create the concave point that initiates tip splitting. The same phenomenon is observed in impure pivalic acid[27] by Bechoefer and Libchaber: close to threshold cell shapes are sufficiently rounded for tip splitting to take place, then, very rapidly because the strong anisotropy of pivalic acid gives more pointed shapes than CBr_4, tip splitting becomes impossible as pulling speed is increased. It also seems that in the experiments reported here the phase-diffusion-type mechanism is blocked: we no longer observe the rapid readjustment illustrated in Fig. 12. Under these conditions cells can only grow larger, hence the anomalously large ones observed.

V. FROM CELLS TO DENDRITES

There is some confusion in the literature as to the exact definition of the term dendrite. We shall call a dendrite any cell that has developed visible sidebranches, i.e., nonstationary, quasiperiodic deformations of its flanks, in practice of a minimum amplitude of 2–3 μm.

The increase in the dispersion in the cell widths described above announces the appearance of dendrites. It is associated with a dispersion in the cell *shapes*. One can observe along a given front the coexistence of narrower rounded cells behaving like the cells described in Sec. III and wider cells that are more pointed. These cells, when reduced to unit width, are no longer superposable. Figure 13 shows the cell widths observed along a given front and photographs of some of the cells. The ratio λ/ρ is no longer constant (Fig. 14) but increases for the larger cells, so that they are no longer homothetic. The profiles of the larger cells fit to a parabola over a greater height (at most 2ρ) and the tip radius tends to become independent of λ as expected in the dendritic regime where ρ is determined only by V. Finally, the largest cells develop sidebranches. With such a large dispersion not only in cell widths—they can vary by a factor 3 along a given front—but also in cell shapes, it becomes quite meaningless to compute an average value of the cell width, one loses too much information on the physical mechanism behind the appearance of sidebranches.

The dispersion in cell widths associated with the appearance of sidebranches can be observed in a number of systems. Trivedi[28] remarked on the coexistence of narrow cells and wider dendrites in the succinonitrile-acetone system, as did Bechhoefer *et al.* in liquid crystals.[29] Published micrographs[30] of Al-Cu show the same phenomenon.

The Péclet number expresses the degree of "interconnection" of the cells through solute diffusion which has a range of the order of the diffusion length. When this length becomes smaller than the cell width (i.e., $P > 1$), the cells should no longer be influenced by each other, and the lateral instability should be free to develop. This notion is confirmed by the numerical calculations of Saito *et al.*[23] We have calculated the Péclet number for the widest cells, P_{cell}, and for the narrowest dendrites, P_{den}, along various fronts (Fig. 15). We find that sidebranches appear for P between 2 and 3 at velocities of 20—30 μm/s and 4–5 at velocities of 50–60 μm/s. This result

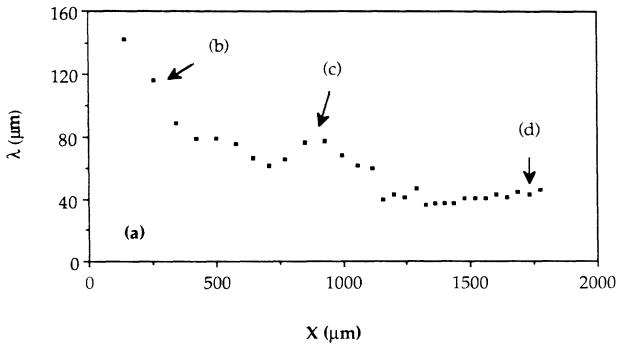

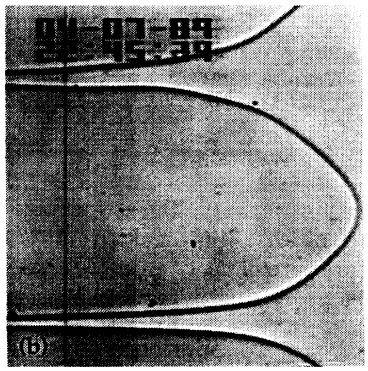

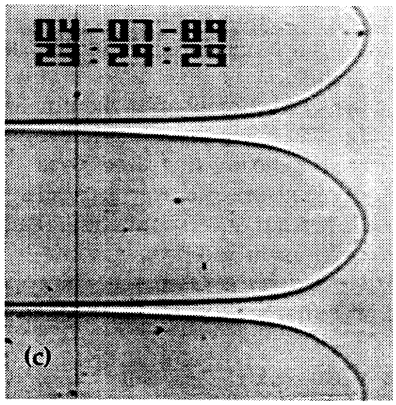

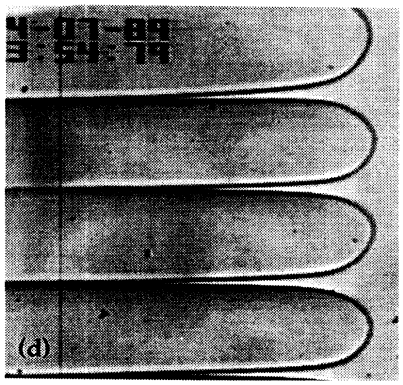

FIG. 13. Cell widths vs their position along the solidification front (a) and photographs of cells at the points indicated on the curve [(b), (c) (d)]. Note the small amplitude sidebranches on (b).

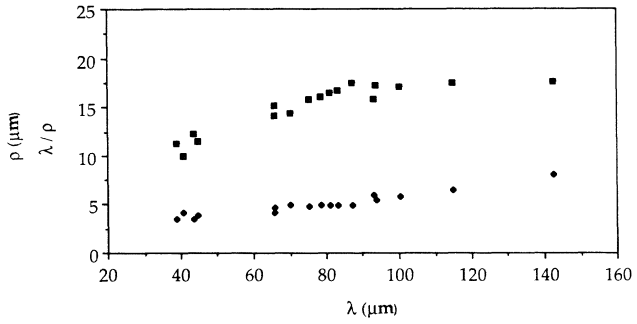

FIG. 14. Tip radius ρ (squares) and reduced curvature λ/ρ (diamonds) vs cell width ($G=46$ K/cm, $V=25$ μm/s, $\epsilon=9$).

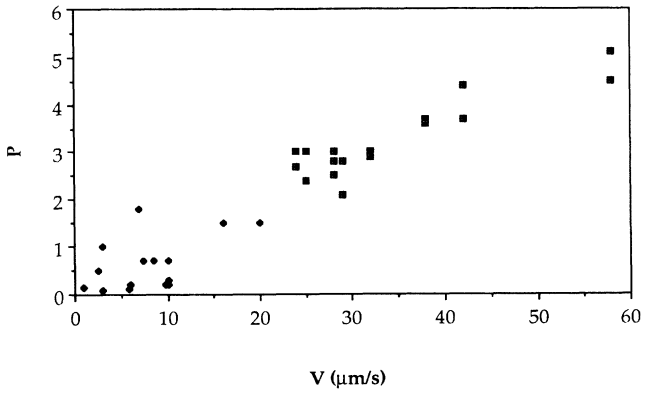

FIG. 15. Péclet numbers for the widest cells (P_{cell}) and the narrowest dendrites (P_{den}) reported, vs pulling velocities. Diamonds represent the values measured in the present experiments and diamonds those indicated in Table I.

can be compared with other experiments when data concerning *individual* cells are available. We calculate the Péclet numbers for the widest cells (P_{cell} at V_{cell}) and for the narrowest dendrites reported (P_{den} at V_{den}), which gives us a more or less well-defined interval. These data appear in Table II and in Fig. 15. In spite of the imprecision, there is a clear tendency for the limiting Péclet number to increase as velocity is increased. Classen *et al.*[31] have shown numerically that the Péclet number at which sidebranches appear increases with increasing kinetic anisotropy. Anisotropy of surface tension on the other hand does not affect it. Figure 15 tends to confirm this result, since kinetic effects increase as velocity increases. The increase in the limiting P can be interpreted qualitatively as being due to the fact that the preferential directions of growth are more sharply defined when strong kinetic effects are present. In the cubic crystals under study here sidebranches must grow perpendicular to the main stem, that is, well back to the sides of the cell. More space is needed than for less anisotropic growth where the branches can begin to grow on the inclined flanks of the cell tips. For low velocities the limiting $P\approx 0.1$. The model of Karma and Pelcé[32] concerning the mechanism for the apparition of sidebranches could be applicable in this regime.

To summarize, a given cell becomes a dendrite once it is sufficiently wide, that is, once P reaches a value that is of order 1 but that increases with the pulling velocity. This limiting value of P can be attained by increasing λ—this is the case in our experiments. Then the appearance of sidebranches on a cell is a *local* phenomenon and when and where this occurs depends on local events (neighboring cells being pinched off). The concept of a sharp and well-defined "cell to dendrite *transition*," frequently used in the literature, is not appropriate here: we do not observe a global transition. The limiting value of P can also be attained by increasing the pulling velocity, as in the experiment of Bechhoefer and Libchaber[27] where wavelength adjustment mechanisms are blocked.

Further experiments on different materials are clearly needed. It will be important to examine the characteristics of individual cells and not only to consider averaged or global quantities. In particular, the increase in the $\bar{\lambda}$

TABLE II. Péclet numbers and pulling velocities for the widest cells and the narrowest dendrites reported in various alloys. (SCN denotes succinonitrile.)

Alloy	P_{cell}	V_{cell} (μm/s)	P_{den}	V_{den} (μm/s)
Impure pivallic acid[a,b]	0.75	10	1.5	20
Pivalic acid—ethanol[c,d]	1	3	1.8	7
SCN acetone[e]	0.5	2.5	0.7	8.5
SCN acetone[c]			0.15	1
Al-4.5 wt. % Cu[f]	0.1	5.8	0.2	9.8
Al-2 wt. % Cu[g]	0.2	10	0.3	10
Al-4.1 wt. % Cu[h]	0.1	3	0.2	6
Fe-8 wt. % Ni[i]	0.7	7.4	1.5	16.1

[a]J. Bechhoefer and A. Libchaber, Phys. Rev. B **35**, 1393 (1987), Fig. 2.
[b]Using $D\approx 10^{-5}$ cm^2/s [J. Bechhoefer, H. Guido, and A. Libchaber, C. R. Acad. Sci. **306**, 619 (1988)].
[c]M. A. Eshelman, V. Seetharaman, and R. Trivedi, Acta Metall. **36**, 1165 (1988).
[d]Using $D=0.4\times 10^{-5}$ cm^2/s [P. Bouissou, Ph.D. thesis, University Paris VII, Paris, France (1989)].
[e]H. Esaka, Ph.D. thesis, Ecole Polytechnique Fédérale de Lausanne, 1986.
[f]An Geying and Liu Lixin, J. Cryst. Growth **80**, 383 (1987).
[g]R. M. Sharp and A. Hellawell, J. Cryst. Growth, **11**, 77 (1971), Fig. 1(b).
[h]Y. Miyata, T. Suzuki, and J. I. Uno, Metall. Trans. **16A**, 1799 (1985).
[i]I. Jin and G. R. Purdy, J. Cryst. Growth **23**, 37 (1974).

versus V curve, often used to define the cell to dendrite transition, probably masks the large dispersion occurring as the cells develop sidebranches.

VI. CONCLUSION

We have observed two different regimes in cellular growth. The first, observed up to relative velocities of approximately 8 produces rounded cells, of well-defined widths, the shape of which only depends on this relative velocity. These shapes are not well predicted by an analogy with Saffman-Taylor fingers. As the constraint is increased, abnormally large cells begin to appear and when their width exceeds 2–3 times the diffusion length ($P \geq 2-3$) they develop sidebranches. The appearance of dendrites is therefore a *local* phenomenon in CBr_4-Br_2 and not a global transition.

ACKNOWLEDGMENTS

We gratefully acknowledge support for this research by the Centre National des Etudes Spatiales, Contract No. 89/CNES/1226. We are indebted to M. BenAmar, B. Caroli, C. Caroli, G. Faivre, C. Misbah, M. Mashaal, B. Perrin, and B. Roulet for fruitful discussions and prior communication of their results.

[1]J. S. Langer, Rev. Mod. Phys. **52**, 1 (1980).
[2]W. W. Mullins and R. F. Sekerka, J. Appl. Phys. **35**, 444 (1964).
[3]C. Normand, Y. Pomeau, and M. G. Velarde, Rev. Mod. Phys. **49**, 581 (1977).
[4]R. C. Diprima and H. L. Swinney, in *Hydrodynamic Instabilities and the Transition to Turbulence*, edited by H. L. Swinney and J. P. Gollub (Springer, Berlin, 1981).
[5]K. A. Jackson and J. D. Hunt, Trans. Metall. Soc. AIME **236**, 1929 (1966).
[6]S. de Cheveigné, C. Guthmann, and M. M. Lebrun, J. Phys. (Paris) **47**, 2095 (1986).
[7]P. Kurowski, Ph.D. thesis, Université Paris VII, 1990.
[8]H. Müller-Krumbhaar (private communication) has characterized them, in reference to European architecture, as "romanesque" and "gothic."
[9]B. Billia, H. Jamgotchian, and L. Capella, J. Cryst. Growth **82**, 747 (1987).
[10]P. G. Saffman and G. Taylor, Proc. R. Soc. London, Ser. A **245**, 312 (1958).
[11]P. Pelcé and A. Pumir, J. Cryst. Growth **73**, 337 (1985).
[12]T. Dombre and V. Hakim, Phys. Rev. A **36**, 2811 (1987).
[13]J. D. Weeks and W. Van Saarloos, Phys. Rev. A **39**, 2772 (1989).
[14]M. Mashaal, M. Ben Amar, and V. Hakim, Phys. Rev. A **41**, 4421 (1990).
[15]S. de Cheveigné, C. Guthmann, P. Kurowski, E. Vicente, and H. Biloni, J. Cryst. Growth **92**, 616 (1988).
[16]Y. Couder, N. Girard, and M. Rabaud, Phys. Rev. A **34**, 5175 (1986); G. Zocchi, B. E. Shaw, A. Libchaber, and L. P. Kadanoff, *ibid.* **36**, 1894 (1987).
[17]J. W. MacLean and P. G. Saffman, J. Fluid Mech. **102**, 455 (1981).
[18]M. Mashaal and M. Ben Amar, in *Patterns, Defects and Material Instabilities*, edited by D. Walgraef and N. H. Ghoniem (Kluwer Academic, Dordrecht, 1990).
[19]L. H. Ungar, M. J. Benett, and R. A. Brown, Phys. Rev. B **31**, 5923 (1985).
[20]M. Ben Amar and B. Moussalam, Phys. Rev. Lett. **60**, 317 (1988).
[21]D. A. Kessler and H. Levine, Phys. Rev. A **39**, 3041 (1989).
[22]Y. Saito, C. Misbah, and H. Müller-Krumbhaar, Phys. Rev. Lett. **63**, 2377 (1989).
[23]Y. Saito, C. Misbah, and H. Müller-Krumbhaar (private communication).
[24]P. Kurowski, S. de Cheveigné, G. Faivre, and C. Guthmann, J. Phys. (Paris) **50**, 3007 (1989).
[25]P. Tabeling, G. Zocchi, and A. Libchaber, J. Fluid Mech. **177**, 67 (1987); see also P. Pelcé, *Dynamics of Curved Fronts* (Academic, New York, 1988).
[26]K. Brattkus and C. Misbah, Phys. Rev. Lett. **64**, 1935 (1990).
[27]J. Bechhoefer and A. Libchaber, Phys. Rev. B **35**, 1393 (1987).
[28]R. Trivedi, Metall. Trans. **15A**, 977 (1984).
[29]J. Bechhoefer, P. Oswald, A. Libchaber, and C. Germain, Phys. Rev. A **37**, 1691 (1988).
[30]R. M. Sharp and A. Hellawell, J. Crystal Growth **6**, 253 (1970); **11**, 77 (1971).
[31]A. Classen, C. Misbah, and H. Müller-Krumbhaar (unpublished).
[32]A. Karma and P. Pelcé, Europhys. Lett. **9**, 713 (1989).

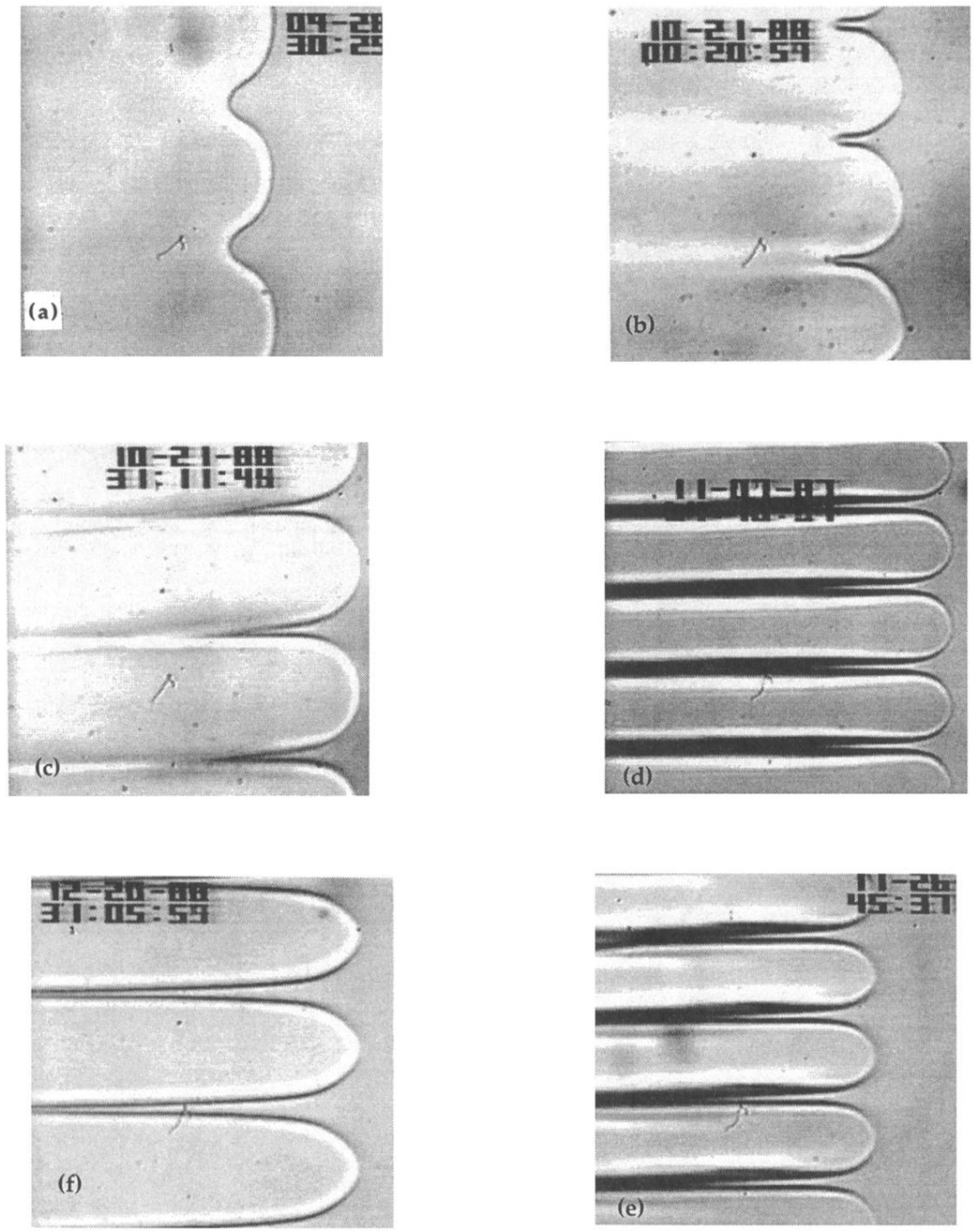

FIG. 1. Cell shapes for different relative velocities: (a) $\epsilon \approx 0.3$ ($V = 7.4$ μm/s, $V_c = 6$ μm/s, $G = 110$ K/cm, $\lambda = 55$ μm, $P = 0.35$); (b) $\epsilon \approx 1.6$ ($V = 14$ μm/s, $V_c = 5.4$ μm/s, $G = 110$ K/cm, $\lambda = 45$ μm, $P = 0.5$); (c) $\epsilon \approx 2$ ($V = 16.6$ μm/s, $V_c = 5.4$ μm/s, $G = 107$ K/cm, $\lambda = 40$ μm, $P = 0.6$); (d) $\epsilon \approx 4$ ($V = 25$ μm/s, $V_c = 5$ μm/s, $G = 106$ K/cm, $\lambda = 30$ μm, $P = 0.6$); (e) $\epsilon \approx 7.5$ ($V = 31$ μm/s, $V_c = 4.1$ μm/s, $G = 100$ K/cm, $\lambda = 30$ μm, $P = 0.8$); (f) $\epsilon \approx 8.5$ ($V = 49.3$ μm/s, $V_c = 5.3$ μm/s, $G = 110$ K/cm, $\lambda = 45$ μm, $P = 1.9$).

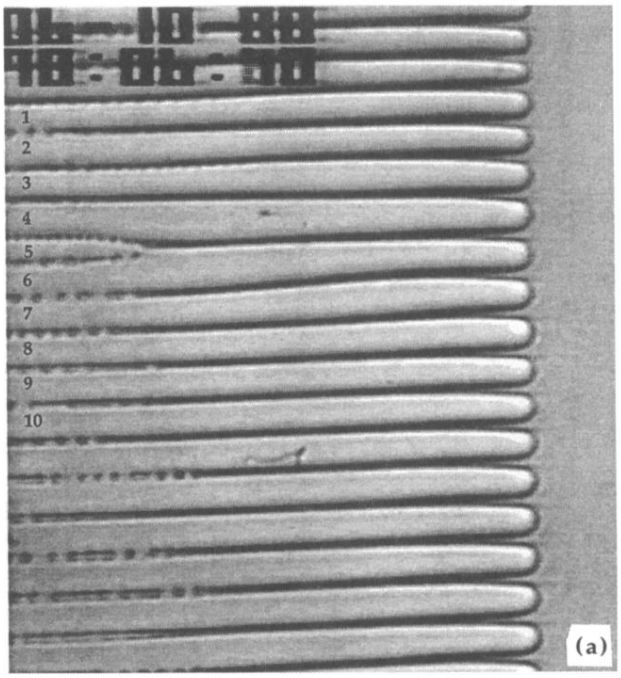

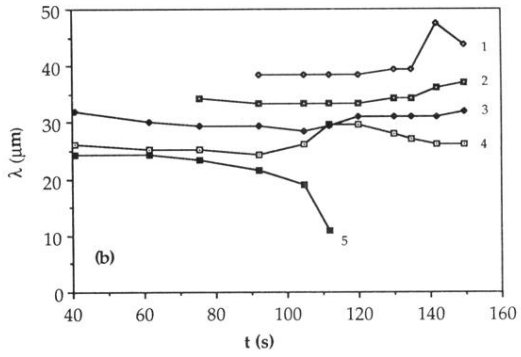

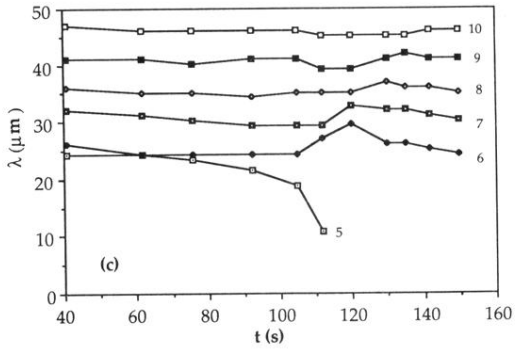

FIG. 12. A cellular front shortly after the pinching off of a cell (a) and (b), (c) the evolution in time of the widths of the cells numbered in Fig. 13(a). Cell number 5 is pinched off at time $t \approx 110$ s. Its neighbors become successively abnormally wide then readjust on a time scale of the order of a minute.

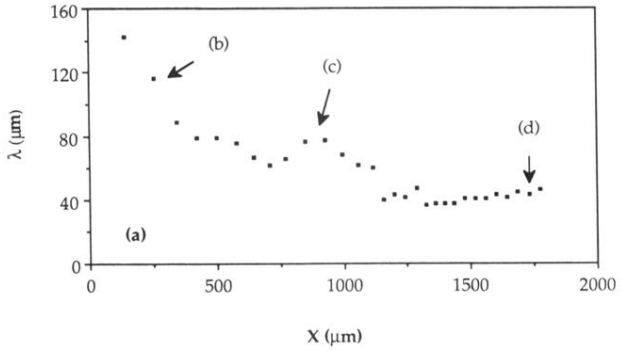

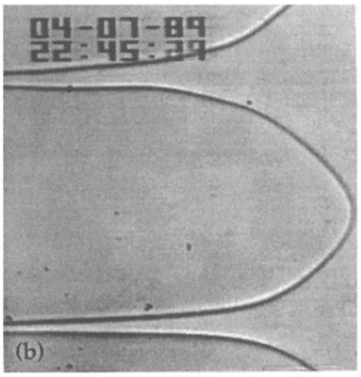

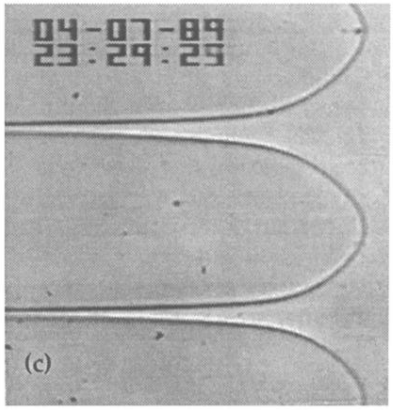

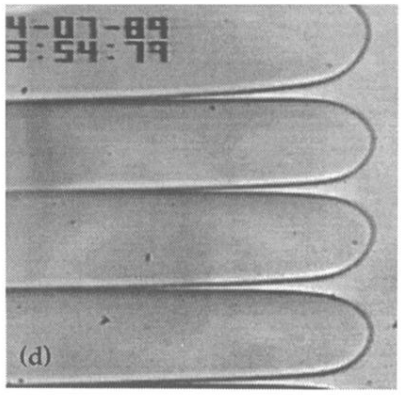

FIG. 13. Cell widths vs their position along the solidification front (a) and photographs of cells at the points indicated on the curve [(b), (c) (d)]. Note the small amplitude sidebranches on (b).